Ain Shams Engineering Journal 15 (2024) 102471

Contents lists available at ScienceDirect

Ain Shams Engineering Journal

journal homepage: www.sciencedirect.com

A multi-functional quasi-single stage bi-directional charger topology for electric vehicles

Burak Tekgun *, Didem Tekgun, Irfan Alan

College of Engineering, Department of Electrical & Electronics Engineering, Abdullah Gul University, Kayseri, Turkey

ARTICLE INFO

Keywords:
EV charger
Multi-functional
Bidirectional
Buck-boost
V2G
V2V

ABSTRACT

In this paper, a multi-functional quasi-single stage, bi-directional electric vehicle charger topology is proposed to realize high efficiency power conversion in all AC/DC, DC/DC, and DC/AC forms. The proposed circuitry includes a noninverting buck boost converter (NBB) and an H-bridge inverter. The NBB converter generates the desired output voltage waveform in the rectified form then the inverter unfolds the waveform to the AC waveform. The advantages of this circuit are the reduced losses due to the high frequency switching only occurring at the NBB converter and passive element sizes are smaller leading to reduced losses and cost. The proposed charger is designed for 2 kVA rating and simulated for all vehicle, grid, and another vehicle interaction modes. Then the circuit is experimentally tested and is validated that the proposed circuit can operate in all three modes at a wide range of loading and power factor conditions with over 92% efficiency.

1. Introduction

Due to the energy demand for transportation increase rapidly worldwide, new technologies regarding to decrease fossil-fuel consumption of the vehicles are becoming more popular recently [1]. As a consequence of the over usage of the fossil fuels, carbon gas emissions are raising up steadily. All-electric and hybrid-electric vehicles (EV) are the area of interest for researchers since they offer a promising solution for reducing the fossil-fuel usage and decrease the greenhouse gas emissions compared to the conventional vehicles. Moreover, many countries such as United States of America, India, China, Finland, and Norway have started to establish new regulations and state their intensions concerning the future of EV sales in automobile industry [2,3]. Therefore, as EV usage are becoming widespread day by day, the energy systems that deal with the related power conversion become critical.

Among the EV batteries, plug-in EV (PEV) and hybrid EV (PHEV) batteries can be charged directly from the electric outlet using on or off-board chargers. Several modes of operations used in EV chargers [4] are Grid-to-Vehicle (G2V), Vehicle-to-Grid (V2G) [5–7], Vehicle-to-Home (V2H) [8,9], Vehicle-to-Load (V2L) [10] and Vehicle-to-Vehicle (V2V) [4] modes which are subject to various research to bring certain flexibility advantages of EVs [11,12] to the forefront. The off-board and portable chargers are also getting attention owing to their substantially lower after-sales maintenance costs in comparison to on-board chargers. [13]. Besides, off-board chargers production cost is obviously lower due to the need to satisfy only the industrial standards rather than the automotive standards [13].

A charger converts the AC mains voltage to various DC voltage magnitudes to satisfy the specific battery requirements. High power density, high efficiency and small size are critical points and essential to obtain an appropriate off-board charger. Currently, EVs chargers' designs are mainly Si-based in industry. EV chargers designed with Si MOSFET can operate in a limited switching frequency range which makes the passive components size larger [14,15]. It is crucial to the switching frequency to be increased to shrink the size of the passive components and obtain high power density to improve the efficiency. However, while working at high switching frequency with Si-based design, there exists excessive losses such as switching losses, conduction losses, core losses and, they cause a significant reduction in efficiency of the charger [16]. Nowadays, with the development of the modern power semiconductor devices like Silicon Carbide (SiC) and Gallium Nitride (GaN) MOSFETs, power converter features are improved, and higher efficiency levels are achieved [17–19]. Recent studies show that power density and efficiency of the chargers increase dramatically with the SiC-based designs [20]. Therefore, SiC MOSFET

Peer review under responsibility of Ain Shams University.

* Corresponding author at: College of Engineering, Department of Electrical & Electronics Engineering, Abdullah Gul University, Sumer Kampusu, Erkilet Blv. 38080, Kocasinan, Kayseri, Turkey.

E-mail addresses: burak.tekgun@agu.edu.tr (B. Tekgun), didem.tekgun@agu.edu.tr (D. Tekgun), irfan.alan@agu.edu.tr (I. Alan).

https://doi.org/10.1016/j.asej.2023.102471
Received 5 December 2022; Received in revised form 27 July 2023; Accepted 2 September 2023
Available online 11 September 2023

Nomenclature

v_{batt}	Battery voltage
i_{batt}	Battery current
C_{in}	Input capacitor, connected parallel to the battery
v_L	DC/DC converter's filter inductor voltage
i_L	DC/DC converter's filter inductor current
L	DC/DC converter's filter inductance
r_L	Series resistance of DC/DC converter's filter inductor
C	DC/DC converter's output filter capacitor
r_C	Series resistance of DC/DC converter's output filter capacitor
v_{rAC}	DC/DC converter's output voltage, which is the rectified form of the output voltage
L_{line}	Line inductance for interfacing AC or DC external systems
v_{out}	Charger output voltage, which is also the interface voltage
i_{out}	Charger output current
D_{buck}	Duty ratio when the DC/DC converter operating as a buck converter
D_{boost}	Duty ratio when the DC/DC converter operating as a boost converter
T	Switching period
t_d	Dead time between two series connected switches when alternate switching
v^*_{out}	Reference output voltage
$v_{ref,rect}$	Rectified form of the reference output voltage
$v_{interface}$	External unit's voltage for interfacing the charger. This value is equal to the charger output voltage when the external unit is connected to the charger
$P_{total\ loss}$	Total power losses of a semiconductor switch
P_{sw}	Switching loss
P_C	Conduction loss
V_{DS}	Drain source voltage of a MOSFET
I_D	Drain current of a MOSFET
f_{sw}	Switching frequency
Q_{GS}	Gate-source charge of a MOSFET
Q_{GD}	Gate-drain charge of a MOSFET
u_{DS}	Voltage drop of a MOSFET
$R_{DS(ON)}$	MOSFET's resistance when turned on
I_{Drms}	RMS diode current
u_D	Diode voltage drop
I_F	Diode forward current
P_{CD}	Diode conduction loss
u_{D0}	Forward voltage drop of a diode
E_{RR}	Reverse recovery energy
i_{RR}	Reverse recovery current of a diode
t_{rr}	Recovering time for reverse recovery
P_{RRD}	Diode reverse recovery loss
P_{SWD}	Total diode loss

technology becomes perfectly suitable for EV chargers to achieve high efficiency, high power density with a smaller size.

Chargers can incorporate several operation modes by processing the power to flow bi-directionally, which refers active power transfer between the EV and another unit such as grid or another EV [21]. The advantages of power sending from vehicle to grid (V2G) are subject to current research since this mode of operation allows to support the power grid or islanded loads in case of an emergency such as natural disasters [22,23]. Beside V2G, V2V power transfer attract the attention of the researchers as it can be critically helpful when an EV is in deep discharge, and it is hard to reach closest charging station. Since it is a fairly new topic, there are limited number of research available in the literature reporting V2V mode of operation. In [24], a SiC based designed on-board EV network with V2V mode is reported where higher efficiency levels are achieved by operating in V2V with DC power transfer through an AC port. In [25], a soft switching interleaved battery charger topology is introduced with high voltage gain as a cost-effective charger alternative. In another study, a multistage approach is introduced for interleaved battery charger [26]. However, these topologies are operating only in charging mode. In [27], two bidirectional on-board chargers are connected to show the power transfer between them. Here, the EVs have to be linked to the DC-link of all battery chargers, which is not practical and hard to implement. A synchronous rectification based three phase 6.6 kW bidirectional CLLC charger topology is proposed in [28] where the input current ripple is tried to be reduced. In [13], a three-phase bi-directional and multifunctional off-board charger is introduced where V2V power transfer operation is done in DC form. Considering the three-phase supply is not available everywhere, this charger structure is not flexible enough to be used in places where only the single-phase supply is available. Among the bidirectional chargers presented above, efficiencies over 96% are achieved for various AC and DC interfacing voltages. For unidirectional chargers, efficiencies exceed 97% as their number of power conversion stages is less.

Although the bi-directional chargers offer a variety of functionalities that are beneficial, the total cost of these systems are higher as the component count increases due to the additional power conversion stages. Moreover, the additional stages can cause reliability problems and could affect the weight and the power density of the EV chargers [29].

This paper presents a modular portable bi-directional buck boost charger that can operate multifunctionally. The proposed charger converts the power for G2V, V2G and V2V in quasi-single stage. Similar charger topologies existing in the literature converts the power either in three or two stages. In all these stages, there exist high frequency switching besides the large number and passive component sizes for filtering. Proposed portable charger topology includes a bidirectional noninverting buck-boost converter (NBB) for generating rectified reference voltages and an H-bridge inverter (HBI) for unfolding. The novelty of this topology which differentiates it from the existing topologies, the high frequency switching is needed only in DC/DC conversion stage, the inverter only unfolds the voltage waveforms when operating in AC output voltage generation modes. Hence, it only switches twice in one period with zero voltage switching action. Moreover, the proposed topology includes a small inductor for the DC/DC conversion stage and a line filter inductor while the existing topologies use expensive large filter inductors to filter the high switching noise. Accordingly, the proposed charger is superior to the others in terms of switching losses, losses associated with the passive filter elements, and the cost. Hence, the proposed charger can work bidirectionally with both DC/AC and DC/DC in a single-phase manner by only switching the controls, which enables the EVs to interact with the on-line and off-line AC grids and other EVs easily and conveniently.

The rest of the paper is organized as follows: Section II presents the interaction modes of the EVs and the power grid. The proposed charger topology, control, and modes of operation are detailed in Section III. The design of the proposed charger and the simulations are given in Section IV followed by the experimental results and discussion. Finally, the paper is concluded with final remarks in Conclusions section.

2. Interaction modes of EVs and grid

The interaction between the AC grid and the EV occurs in two ways namely grid to vehicle for charging and vehicle to grid for supporting the grid to provide reliable and stable operation. In addition to these

interactions, recently vehicle to vehicle interaction for rescuing deeply discharged EVs become an attractive research area [13]. To operate in all these modes, a converter should be able to process the power in both directions and convert the power in DC and AC forms.

2.1. Grid to EV (G2V)

In this operating mode, the power is taken from the grid in AC form and converted to the DC form to charge the batteries of the EVs as shown in Fig. 1.a. Depending on the manufacturer, the charger is composed of two or three power conversion stages.

2.2. EV to grid (V2G)

EV to Grid operating mode is mostly used for stabilizing the grid and improving its reliability. Also, this mode is used for supplying small electric loads in urgent situations such as natural disasters. Basically, the power is taken from the EV battery packs, converted into AC, and pushed back to the grid as shown in Fig. 1.a.

2.3. Vehicle to vehicle (V2V)

EV to EV operating mode is employed when an EV goes into a deep discharge and needs to have an external source to store enough energy to work and drive somewhere safe. This mode is usually realized by converting the DC battery voltage into a higher DC level, then, from this DC level to the AC in the rescued EV and the power in AC form is converted into DC and an additional DC conversion takes place to bring the DC voltage level to the battery voltage level of EV rescued as shown in Fig. 1.b. This four-level power conversion degrades the V2V energy flow process efficiency by having additional losses in each stage. Furthermore, some manufacturers use three stage charger structures in their onboard or portable chargers. In such a case, V2V energy transfer takes place in six stages which in turn causes more losses in rescue operations.

Rather than transferring the energy in AC form in V2V operation, power can be delivered in DC form as shown in Fig. 1.c to avoid additional switching losses during the additional stages. After all, batteries require DC voltage to be charged.

3. Proposed modular Bi-Directional Buck-Boost EV charger

3.1. Circuit topology

Proposed charger topology is realized with a DC/DC converter and an unfolding circuit. While the DC/DC converter generates the rectified reference voltage waveform, the unfolding circuit only switches twice to determine the output voltage polarity in one period. As a result, DC/DC power conversion stage is the only stage that has the switching losses. The unfolding circuit switching instants are where the output voltage crosses zero. Therefore, the switching losses in the unfolding circuit can be considered zero, while the conduction losses still exist in the unfolding circuit. As a result of this approximation, the circuit size got smaller, topology became much simpler than the two/three stage topologies that considered to be conventional, and control of the circuit got simpler.

The selection of the DC/DC converter type is merely depending on the application requirements, it can be buck, boost, buck-boost, or the isolated versions of these converters. In this work, non-isolated, NBB converter structure is employed as the DC/DC conversion unit as shown in Fig. 2.a considering its symmetrical structure and simple control features.

This circuit can operate bi-directionally with AC or DC voltage (Fig. 2.b) depending on the interface voltage. The design of the circuit consists of the filter inductor and capacitor selection based on the circuit operating modes and interface inductor selection based on the current THD limitations. The process of selecting appropriate filter elements presents a challenging task due to constraints imposed by the IEEE standards on limiting output current THD [30]. Additionally, NBB operation exhibits variability in response to changes in pf and load conditions, potentially resulting in the selected filter elements failing to achieve the desired THD levels. A comprehensive examination of this issue can be found in the authors' prior works [31,32].

During the selection of the filter elements, continuous conduction mode operation is aimed in boost mode and discontinuous conduction mode in buck mode where the output voltage gets close to the zero values. This way, undesired voltage peaks during the zero crossings do not occur as it is a common problem of the similar circuit topologies that use unfolding circuits. Besides, the circuit can operate in a wide range of power factor (pf) conditions with a good signal quality.

3.2. Control

The proposed charger uses an open-loop structure while generating the gating signals just like a voltage source inverter (VSI). The reference voltage that is calculated by a higher-level controller. First, the sign of the reference is determined; hence, switches Q_5, Q_6, Q_7, and Q_8 are turned on and off accordingly. The absolute value of the reference voltage is normalized to control the bi-directional DC/DC converter. The NBB's conversion ratio is defined by the normalized reference signal. For instance, if the ratio is less than one, the converter is stepping down, or if it is greater than one the converter is stepping up the voltage linearly. The switches Q_1 and Q_2 are controlled with the normalized reference signal that is limited between zero and one and the duty ratio is calculated with the following expression.

$$D_{buck} = \frac{V_o}{V_i} \tag{1}$$

To control the switches Q_3 and Q_4, the normalized reference is fed to a lookup table (LUT) for linearizing the operation in boost mode. The LUT simply calculates the duty ratio of the boost mode switch using the following expression.

$$D_{boost} = \frac{V_o - V_i}{V_o} \tag{2}$$

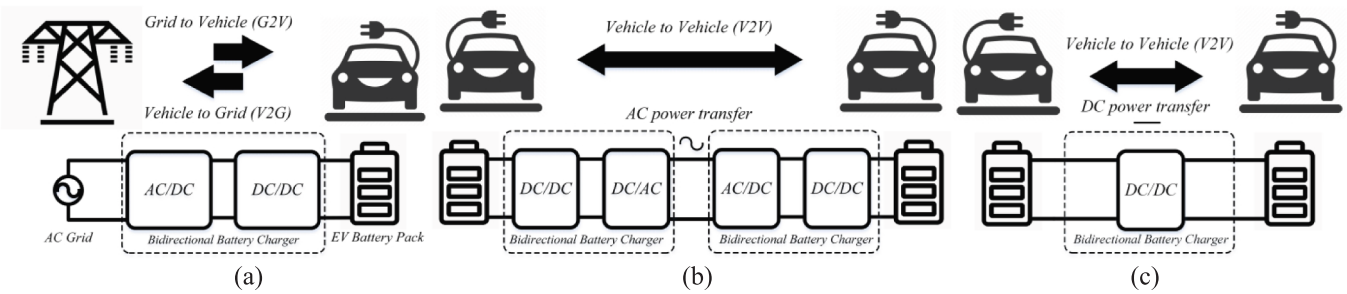

Fig. 1. (a) G2V and V2G operation modes, (b) conventional V2V operation with AC Power, (c) V2V operation with DC power.

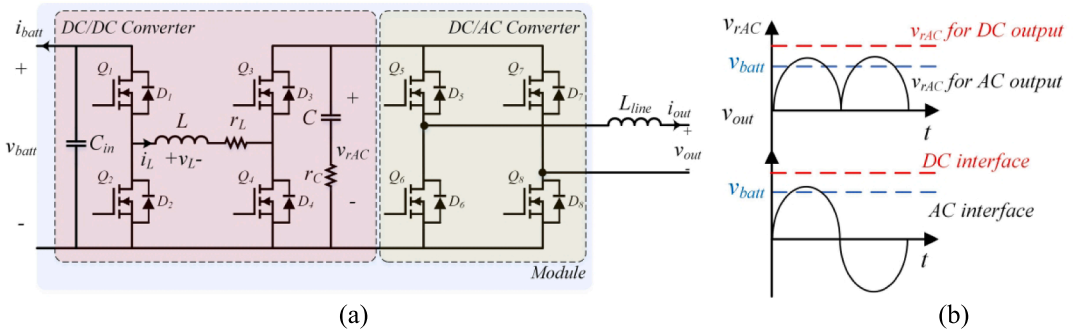

Fig. 2. (a) Proposed modular bi-directional buck-boost charger and (b) related voltage waveforms.

The control system block diagram and the duty ratio versus conversion ratio plots are presented in Fig. 3.a. The limit for the conversion ratio is selected as 3 for safe and stable operation.

The higher-level controller mentioned above is a controller that manages the energy flow and determines the reference voltage for the interface terminal based on the operation mode. Mode selection, active and reactive powers reference selection for V2G and G2V modes, and current reference selection in V2V mode can be done by either the vehicle control unit or manually within the hardware limits. This control structure is presented in Fig. 3.b and Fig. 3.c.

In Fig. 3.b, the power is controlled through current. In both G2V and V2G operating modes, the controller structure is the same. Typically, the pf is kept unity when charging the batteries; however, to use the EVs for grid stabilization or reactive power compensation during the charging and discharging, it is required for the charger to have the ability to produce or consume reactive power, too. Therefore, depending on the operational scenario, some amount of reactive power can be given to the system as a reference. During the charging, constant current (CC) and constant voltage (CV) operation modes selection decision is left to the vehicle control unit. In V2V mode, since the intension is to rescue an EV that is deeply discharged, only CC mode is implemented as shown in Fig. 3.c.

3.3. Circuit modes of operation

The NBB converter is operated in four modes, charging, and discharging with boost and buck modes. The operating modes of circuit when the power is flowing from the input to the output (discharging) as in V2G and V2V modes are shown in Fig. 4.

During discharging (red lines in Fig. 4), when the NBB runs in buck mode, Q_3 transistor is turned on and Q_4 is turned off, and Q_1 and Q_2 transistors are alternated. The switching function, voltage and current of the inductor are presented in Fig. 4.a. For the same operating condition, the circuit modes for different time intervals are presented in Fig. 4.b, Fig. 4.c, and Fig. 4.d. During discharging (red lines in Fig. 4), when the NBB runs in boost mode, the Q_1 transistor is turned on, Q_2 is turned off; the Q_3 and Q_4 transistors alternately switch for NBB to operate as boost converter. The switching function, voltage and current of the inductor

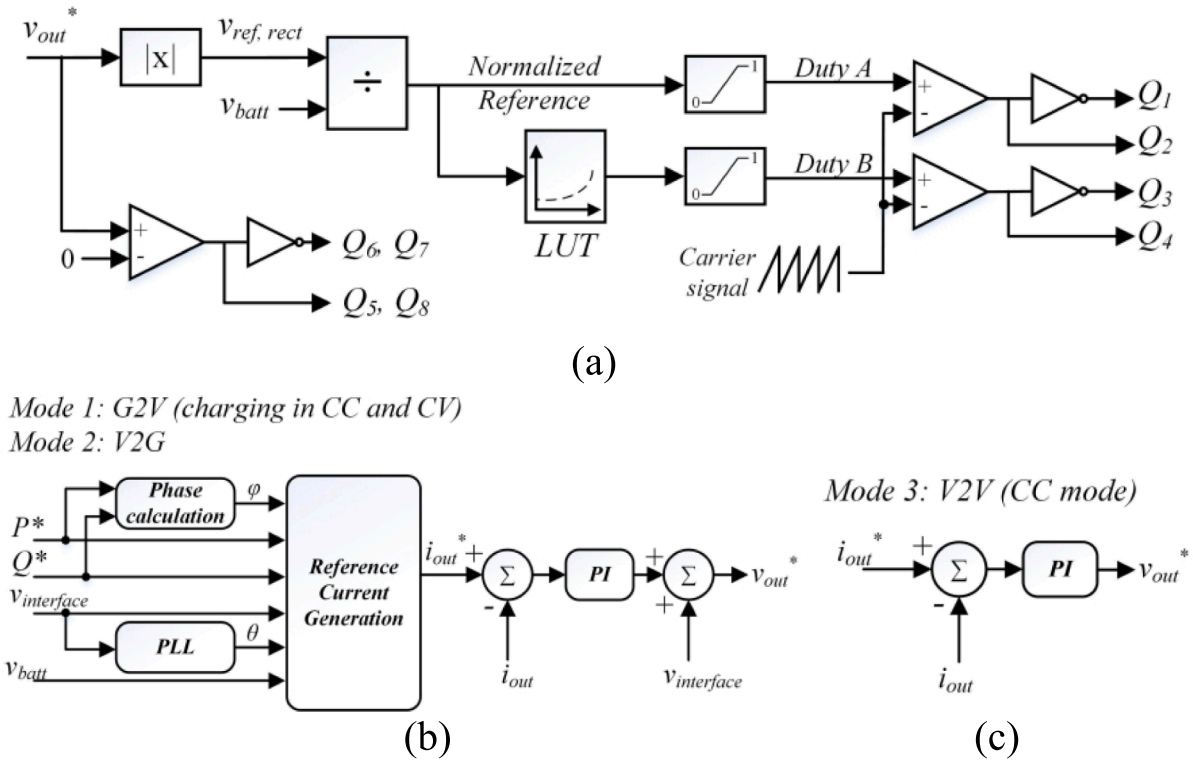

Fig. 3. (a) The voltage control scheme of the proposed charger and duty cycles of the Q_1 (Q_2 alternates) and the Q_3 (Q_4 alternates) switches vs. the normalized voltage reference; (b) The output current controller in G2V, V2G, and (c) V2V operation modes.

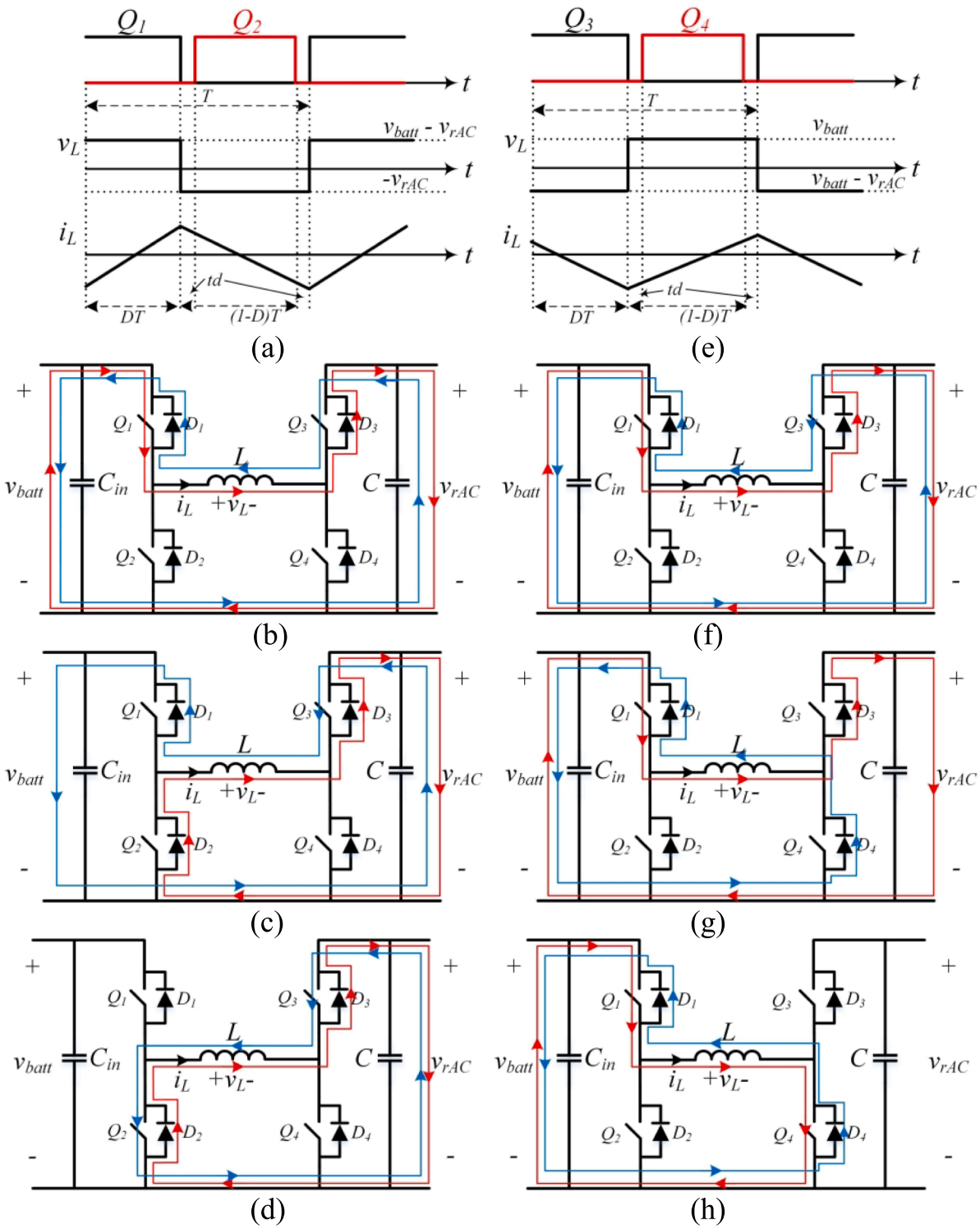

Fig. 4. During discharging (red lines) when NBB operates in buck mode: (a) the switching function, the voltage, and current of the inductor, and the circuit modes for (b) $0 < t < DT$, (c) $DT < t < DT + t_d$, and (d) $DT + td < t < T$; when NBB operates in boost mode: (e) the switching function, the voltage, and current of the inductor, and the circuit modes for (f) $0 < t < DT$, (g) $DT < t < DT + td$, and (h) $DT + td < t < T$. (For interpretation of the references to colour in this figure legend, the reader is referred to the web version of this article.)

are presented in Fig. 4.e. The circuit modes for the boost operation for different time intervals are provided in Fig. 4.f, Fig. 4.g, and Fig. 4.h.

Similarly, the charging (G2V) mode work with the buck and boost modes, too. Here, the control is flipped due to the NBB converter's symmetrical structure. Hence, no further explanation is presented for G2V.

3.4. Losses

Power losses in semiconductor devices can be divided into three groups: conduction (P_c), switching (P_{sw}), and leakage losses. Generally, the leakage losses are small enough to be neglected. Hence, the total power losses of a semiconductor can be calculated as:

$$P_{totalloss} = P_{sw} + P_c \tag{3}$$

In each switching electrical cycle, semiconductors have turn-on, and turn-off losses. The rise time and fall time values along with the switch turn-on and turn-off charge data is available in datasheets. Thus, the switching losses of a MOSFET can be calculated by [33].

$$P_{sw} = V_{DS} I_D f_{sw} \left(\frac{Q_{GS} + Q_{GD}}{I_G} \right) \tag{4}$$

where V_{DS} is the drain-source voltage of the MOSFET, I_D is the drain current, f_{sw} is the switching frequency, Q_{GS} and Q_{GD} are the gate to source and gate to drain charges, and I_G is the gate current.

The on-state resistance of a MOSFET switch, $R_{DS(ON)}$, and total gate charge, Q_G are the key parameters that determine the switching speed and energy. The large Q_G causes slow switching speed and high switching losses while the high $R_{DS(ON)}$ causes high voltage drop and high conduction losses. The voltage drop in semiconductor is expressed as in (5).

$$u_{DS} = R_{DS(ON)} I_D \tag{5}$$

Here, $R_{DS(ON)}$ is a function of temperature and the drain current where the related information is available in datasheets. The average conduction loss in a MOSFET can be calculated as follows.

$$< P_c >= \frac{1}{T_{sw}} \int_0^{T_{sw}} P_c dt = R_{DS(ON)} I_{Drms}^2 \tag{6}$$

Each MOSFET in the proposed circuit has an anti-parallel diode connected in parallel and these diodes also contribute to losses. The anti-parallel diode voltage drop can be obtained as in (7).

$$u_D = u_{D0} + R_D I_F \tag{7}$$

Here, R_D is internal resistance of the diode and u_{D0} is forward voltage drop. Similarly, the average conduction loss of the anti-parallel diode can be expressed as in (8).

$$P_{CD} = u_{D0} I_{Fav} \tag{8}$$

where I_{Fav} is the average diode current. Diodes also introduce losses during the turn-off process called reverse recovery loss, P_{RRD}. This loss is a function of the forward current, higher forward current leads a higher reverse recovery current, i_{RR}, and recovering time, t_{RR}. The integral of the diode's reverse recovery current and the voltage multiplication over the recovering time gives the reverse recovery energy, E_{RR}, that is used to calculate this loss as following.

$$E_{RR} = \int_0^{t_{RR}} i_{RR} V_D dt \tag{9}$$

$$P_{RRD} = E_{RR} f_{sw} \tag{10}$$

Hence, the total loss on the anti-parallel diode, P_{SWD}, is expressed as in (11).

$$P_{SWD} = P_{CD} + P_{RRD} \tag{11}$$

In this study, C3M0065090D SiC MOSFET from Cree is used and parameters are presented in Table 1.

Table 1
C3M0065090D sic power mosfet parameters.

Drain-Source Voltage (V_{DS})	900 V	Gate to Source Charge, Q_{GS}	9 nC
Continuous drain current, I_D (A)	36 A	Gate to Drain Charge, Q_{GD}	13 nC
On-time resistance, $R_{DS(ON)}$	65 mΩ	Total gate charge, Q_G	35 nC
Turn-On Switching Energy, E_{ON}	343 μJ	Output capacitance, C_{OSS}	66 pF
Turn Off Switching Energy, E_{OFF}	46 μJ	Peak reverse recovery current, $i_{RR,max}$	8 A
Diode Forward Voltage, V_D	4.4 V	Reverse recovery time	26 ns

4. Design and simulations

In this section, the proposed charger is designed and simulated to validate the operational capabilities. The case study is conducted using the system specifications given in Table 2.

The current ripple for the voltage boost and buck operations are selected as 100% and 125%, respectively. Since the converter can operate at various pf conditions, the ripple is selected based on the unity pf condition. Having such high current ripple values are the result of the proposed charger to be able to process power at a wide range of pf conditions. The converter operates at discontinuous current mode when operating in buck mode close to the voltage zero crossings, whereas operates in continuous conduction mode in boost mode. Considering the limitations, the inductor and the output capacitor values are determined as 50 μH and 4 μF. The inductive line filter placed between the charger and the grid is selected as 2 mH to avoid current inrushes and to provide a low total harmonic distortion (THD) current. The capacitor connected parallel to the battery is selected as 5 mF to limit the voltage variation to 5% of the rated voltage. The simulations are done in PSIM platform. For both charging and discharging operations, the rated apparent power is set to 2 kVA. It should be kept in mind that only the active power is charging the battery when charging, and active power is drawn from the battery when discharging. Fig. 5.a and Fig. 5.b show the instantaneous output current, battery current, output voltage, battery voltage, voltage before the H-bridge inverter, and the inductor current waveforms of G2V mode at 2 kVA charging condition with unity and 0.8 pf conditions. Fig. 5.c and Fig. 5.d show the same instantaneous current and voltage waveforms for V2G mode at 2 kVA discharging condition with unity and 0.8 pf conditions.

In V2V rescue mode, the interface voltage between two EVs is a DC voltage and selected as 300 V which is within the safe operation limits as the vehicle charging port can operate up to 1000 V with 50 A current. Fig. 5.e shows the instantaneous battery current and voltage, the voltage before the H-bridge inverter, the output voltage, output current, and the inductor current waveforms. It can be seen from the figure that the charging current ripple is negligibly small.

Fig. 5.f shows the loss distribution of G2V, V2G, V2V modes at 2 kW where the grid and battery voltages are 220 V_{AC} and 200 $V_{DC,}$ respectively. The AC current is 10 A_{rms} with unity pf for the G2V and V2G modes. The losses are grouped as transistor switching and conduction losses, $P_{SW(Q1\text{-}Q4)}$, and $P_{C(Q1\text{-}Q4)}$, H-bridge conduction loss (includes both transistor and diode conduction loss for different modes) P_{CH}, diode reverse recovery losses and conduction losses, $P_{RRD(D1\text{-}D4)}$, $P_{CD(D1\text{-}D4)}$, NBB inductor conduction loss, P_{CL}, and the line inductance conduction loss, P_{CLine}. The core losses of the inductors are neglected. As seen from the Fig. 5, in G2V mode, the H-bridge conduction loss is quite high as the input current pass through two diodes. Similarly, the conduction loss of the D_1-D_4 switches is high compared to other loss components as diodes keep fairly high forward voltage during conduction.

5. Experimental results

The proposed charger and its operating modes are verified through a set of experiments. 65 mΩ discrete SiC Mosfets are used in all stages, all the filter parameters are kept the same with the simulations. The NBB

Table 2
System specifications.

Parameter	Value
Battery voltage	200 V
Grid voltage	220 V_{RMS}, 50 Hz
Rated output power	2 kVA
Converter operating frequency	100 kHz

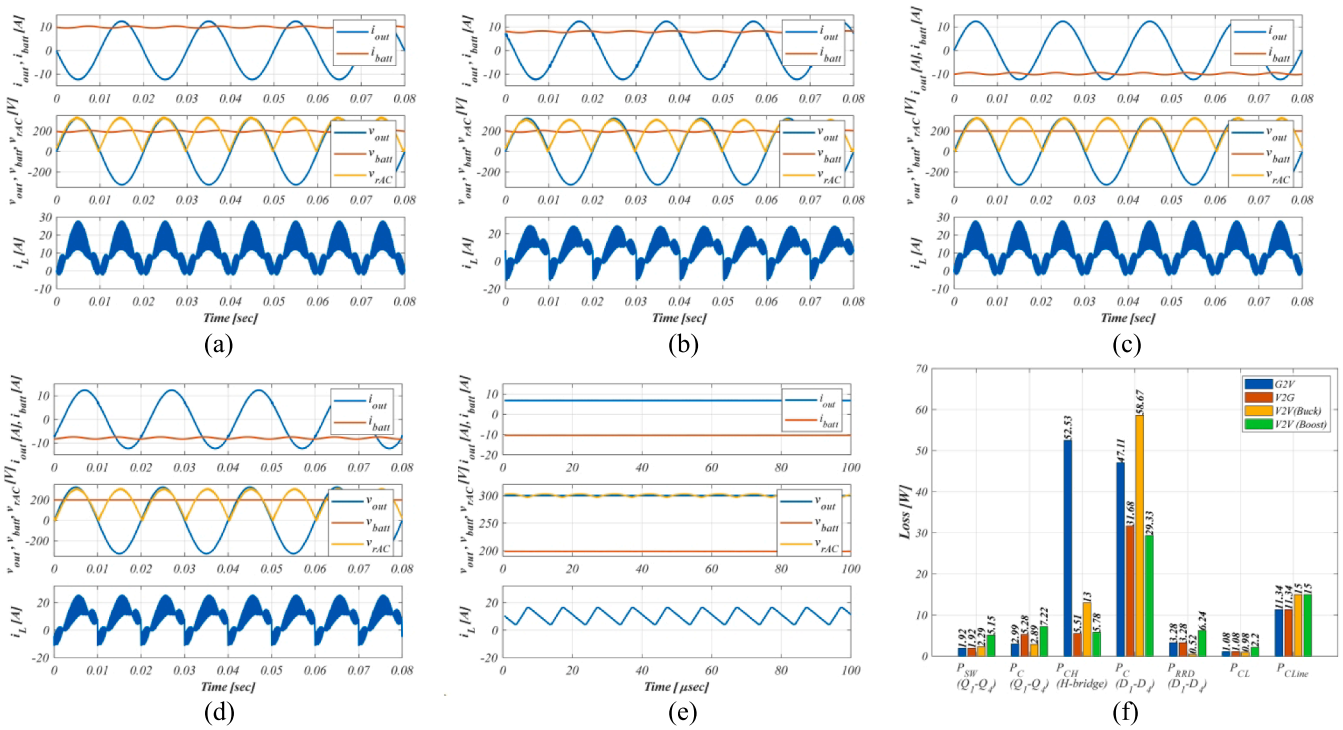

Fig. 5. Current and voltage waveforms of G2V mode at 2 kVA charging condition with (a) unity and (b) 0.8 pf; V2G mode at 2 kW charging condition with (c) unity and (d) 0.8 pf conditions, and (e) the output, inductor, battery current waveforms in V2V rescue mode, and (f) loss distribution in different modes.

converter is operated at 100 kHz, the HBI switches are switched at 100 Hz as the fundamental grid frequency is 50 Hz. A Texas Instruments DSP microcontroller TMS320F28379D is used to control the operation with a sampling time of $T_S = 10$ μs. The battery pack voltage V_{bus} is 200 V. Connection diagrams used for G2V and V2G operation, and V2V operation are given in Fig. 6.a and Fig. 6.b, respectively. The complete test system is presented in Fig. 6.c. The test system includes differential voltage probes, current probes, an oscilloscope, and a bidirectional DC supply acting as a battery pack. The experiments are done for all operating modes including the charging from the grid (G2V), supplying power to the grid (V2G), and supplying to another EV in rescue mode (V2V). The G2V and V2G modes are interfacing the grid and processing the power in AC form while in the V2V mode the power is processed in DC form.

In G2V (charging) mode the power is drawn from the grid pushed into the batteries. During this operation, one can use the proposed charger with unity pf as well as varying pf for grid stabilizing purposes. Fig. 7.a and Fig. 7.b show the proposed circuit operating in charging mode, drawing 2 kVA power from the grid with unity and 0.8 pf, respectively. The battery voltage and the charging current are also presented in the Fig. 7. For unity pf condition, the active and reactive powers are commanded as negative 2 kW and 0 VAr. The battery current

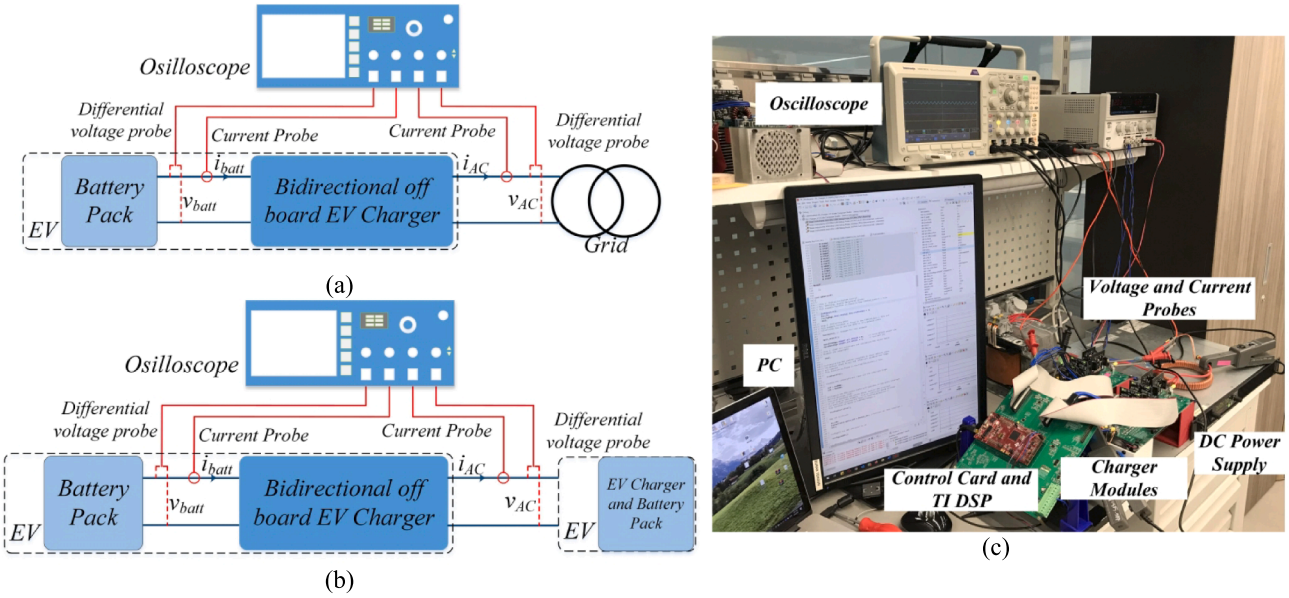

Fig. 6. (a) Connection diagrams used for G2V and V2G operation, (b) V2V operation, and (c) the complete test system.

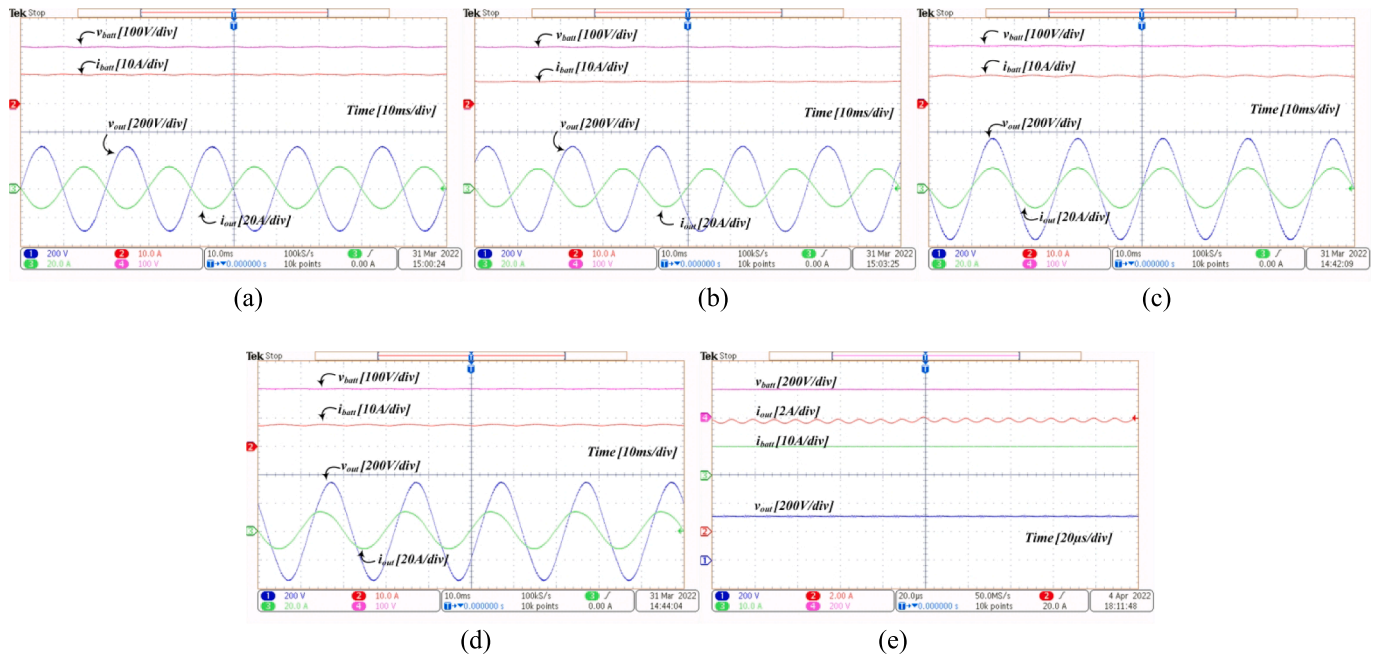

Fig. 7. In G2V (charging) mode, waveforms (a) when the pf is unity and (b) pf is 0.8 at 2 kVA. In V2G (regenerating) mode, waveforms (c) when the pf is unity and (d) pf is 0.8 at 2 kVA. In V2V (rescue) mode, (e) waveforms with DC power transfer at 2 kW.

is recorded as 10 A, considering the battery voltage is 200 V, the charging power is 2 kW. When the pf is 0.8, the active and reactive powers are negative 1.6 kW and 1.2 kVAr, and the battery current is 8 A, which makes the charging power 1.6 kW. It can also be seen that for all pf conditions, the sinusoidal current waveform is maintained.

In V2G mode the power is pushed to the grid from the batteries. Similarly, it is possible to use the proposed charger with unity pf and varying pf for grid stabilizing purposes. Fig. 7.c and Fig. 7.d show the proposed circuit operating in regenerating mode, supplying 2 kVA power to the grid with unity and 0.8 pf, respectively. The battery voltage and the discharging current are shown in the figures. In this mode, the power flows in the opposite direction. Hence, the active and reactive powers are commanded as positive 2 kW and 0 VAr, and the battery current is about 10 A on the opposite direction, the output power is 2 kW. When the pf is 0.8, the active and reactive powers are 1.6 kW and 1.2 kVAr, and the battery current is about 8 A, the output power is 1.6 kW. Similar to the charging mode, for all pf conditions, the sinusoidal current waveform is maintained.

In V2V (rescue) mode experiments, the connection diagram given in Fig. 6.b is used. Rather than transferring the power in AC form, it is transferred in DC form, the voltage, and current waveforms of one of the modules that provide 2 kW power are presented in Fig. 7.e. Here, when the interface voltage is DC 300 V, the output current is commanded as DC 6.7 A for charging the external unit with 2 kW power.

Measured efficiency versus the loading condition of the G2V and V2G modes with 0.7 to unity pf conditions are presented in Fig. 8.a and 8.b. The efficiency of the proposed circuit decreases as the pf decrease. This is due to the apparent power is kept constant while the pf is changing, leading to the switching and conduction losses vary slightly as the charging current amplitude stays the same. Hence, the output active power is reduced. A similar trend is also observed when the charger is regenerating from the batteries to the grid. Over 92% efficiency at a wide range of loading and pf conditions is achieved with the proposed charger topology.

As modern EVs having both AC and DC charge plugs, they are not necessarily charged via only AC, while DC charging is more efficient. In DC power transfer mode, the variable parameter is the battery pack voltage that varies from one manufacturer to other manufacturers. Hence, the experiments conducted with V2V rescue mode, are realized for 3 different DC interface voltages, 150 V, 300 V, and 450 V. When operating at 150 V, the NBB converter operates in buck mode while it operates in boost mode at 300 and 450 V as in our case the first battery pack voltage is 200 V.

The efficiency versus the loading curves for all three DC voltage levels along with the efficiency curve when the interface is 220 V, 50 Hz AC voltage are given in Fig. 8.c. The overall efficiency reaches up to 96% at full load with the DC power transfer while it can barely exceed 91% in AC power transfer as there are four power conversion stages. When the results are compared to the similar bi-directional buck-boost charger studies in literature, the efficiency levels of the proposed topology are

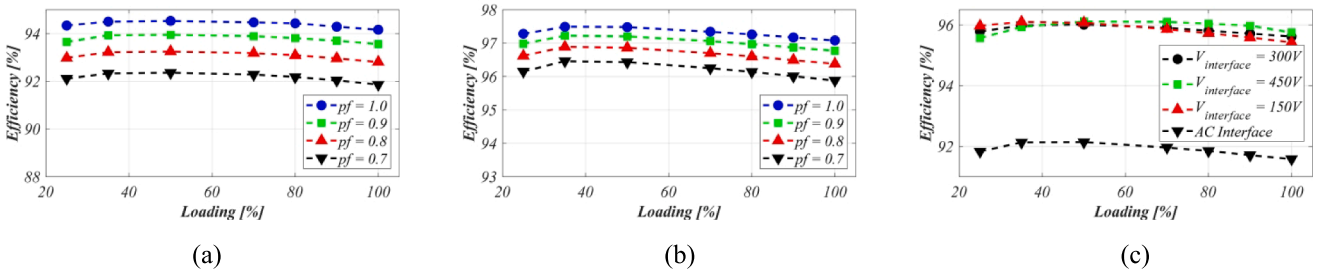

Fig. 8. Efficiency of the (a) G2V and (b) V2G modes at various loading conditions with the pf varying between 0.7 and unity; (c) V2V rescue mode versus the loading.

sufficiently high, even superior for some cases.

6. Conclusion

In this paper, a multi-functional, bi-directional, quasi-single stage, single-phase charger topology is proposed for electric vehicle charging applications. The proposed topology is able to process the power in both directions in AC and DC forms providing a multi-functional operating capability including grid to vehicle, vehicle to grid, and vehicle to vehicle operations. Moreover, the charger can step up and down the voltage in both power flow directions. The proposed charger includes a non-inverting buck-boost (NBB) converter and an H-Bridge inverter (HBI). The NBB converter can operate bi-directionally and generate the desired output voltage waveform in rectified form with high efficiency and the HBI unfolds this signal to form the original AC voltage waveform on the output. This way, the high frequency switching is only needed in DC/DC converter while the unfolding process make the HBI switch only twice over one period when the voltage is zero. The same topology is also useful when the power is transferred from one EV to another one. The power can be converted with both AC and DC interfacing voltage. The proposed charger circuit is designed, simulated, and all the operating modes are experimentally tested. In contrast to similar multi-functional charger topologies documented in the existing literature, the proposed topology exhibits notably elevated levels of efficiency, surpassing 97% in certain instances and consistently maintaining high performance across a broad range of loading conditions. For the worst case when operating in V2V mode with AC interface voltage, the efficiency is recorded as 92%. Future work may include a three-phase structure of the proposed charger topology with wider pf operation capability.

Declaration of Competing Interest

The authors declare that they have no known competing financial interests or personal relationships that could have appeared to influence the work reported in this paper.

References

[1] Kim D-H, Kim M-J, Lee B-K. An integrated battery charger with high power density and efficiency for electric vehicles. IEEE Trans Power Electron 2017;32:4553–65. https://doi.org/10.1109/TPEL.2016.2604404.

[2] International Energy Agency. Global EV Outlook 2018. Global EV Outlook 2018; 2018(79):625–33. https://doi.org/10.1787/9789264278882-en.

[3] International Energy Agency. Global EV Outlook 2023. OECD 2023. https://doi.org/10.1787/cbe724e8-en.

[4] Hsu Y-C, Kao S-C, Ho C-Y, Jhou P-H, Lu M-Z, Liaw C-M. On an electric scooter with G2V/V2H/V2G and energy harvesting functions. IEEE Trans Power Electron 2018; 33:6910–25. https://doi.org/10.1109/TPEL.2017.2758642.

[5] Kisacikoglu MC, Ozpineci B, Tolbert LM. EV/PHEV Bidirectional charger assessment for V2G reactive power operation. IEEE Trans Power Electron 2013;28: 5717–27. https://doi.org/10.1109/TPEL.2013.2251007.

[6] de Melo HN, Trovao JPF, Pereirinha PG, Jorge HM, Antunes CH. A controllable bidirectional battery charger for electric vehicles with vehicle-to-grid capability. IEEE Trans Veh Technol 2018;67:114–23. https://doi.org/10.1109/TVT.2017.2774189.

[7] Wang M, Craig MT. The value of vehicle-to-grid in a decarbonizing California grid. J Power Sources 2021;513:230472. https://doi.org/10.1016/j.jpowsour.2021.230472.

[8] Yongsheng Fu YHH (Kevin) BXLKZ and CC. A High-efficiency SiC Three-Phase Four-Wire inverter with Virtual Resistor Control Strategy Running at V2H mode. 2018 IEEE 6th Workshop on Wide Bandgap Power Devices and Applications (WiPDA), 2018, p. 174–9. https://doi.org/978-1-5386-5909-0/18.

[9] Kwon M, Choi S. An electrolytic capacitorless bidirectional EV charger for V2G and V2H applications. IEEE Trans Power Electron 2017;32:6792–9. https://doi.org/10.1109/TPEL.2016.2630711.

[10] Wang X, Liu Y, Qian W, Janabi A. Design, and control of a SiC isolated bidirectional power converter for V2L applications to both DC and AC load. In: IEEE 7th Workshop on Wide Bandgap Power Devices and Applications (WiPDA); 2019. p. 143–50.

[11] Wickramasinghe Abeywardana DB, Acuna P, Hredzak B, Aguilera RP, Agelidis VG. Single-phase boost inverter-based electric vehicle charger with integrated vehicle to grid reactive power compensation. IEEE Trans Power Electron 2018;33: 3462–71. https://doi.org/10.1109/TPEL.2017.2700944.

[12] Zhang L, Brown T, Samuelsen S. Evaluation of charging infrastructure requirements and operating costs for plug-in electric vehicles. J Power Sources 2013;240:515–24. https://doi.org/10.1016/j.jpowsour.2013.04.048.

[13] Wang S, Li H, Zhang Z, Li M, Zhang J, Ren X, et al. Multi-function Capability of SiC Bidirectional Portable Chargers for Electric Vehicles. IEEE J Emerg Sel Top Power Electron 2021. https://doi.org/10.1109/JESTPE.2021.3052841.

[14] Zhang Z, Yao K, Ke G, Zhang K, Gao Z, Wang Y, et al. SiC MOSFETs Gate driver with minimum propagation delay time and auxiliary power supply with wide input voltage range for high-temperature applications. IEEE J Emerg Sel Top Power Electron 2020;8:417–28. https://doi.org/10.1109/JESTPE.2019.2951358.

[15] Shi C, Wang H, Dusmez S, Khaligh A. A SiC-based high-efficiency isolated onboard PEV charger with ultrawide DC-link voltage range. IEEE Trans Ind Appl 2017;53: 501–11. https://doi.org/10.1109/TIA.2016.2605063.

[16] Whitaker B, Barkley A, Cole Z, Passmore B, Martin D, McNutt TR, et al. A high-density, high-efficiency, isolated on-board vehicle battery charger utilizing silicon carbide power devices. IEEE Trans Power Electron 2014;29:2606–17. https://doi.org/10.1109/TPEL.2013.2279950.

[17] Zdanowski M, Peftitsis D, Piasecki S, Rabkowski J. On the design process of a 6-kVA Quasi-Z-inverter employing SiC power devices. IEEE Trans Power Electron 2016;31:7499–508. https://doi.org/10.1109/TPEL.2016.2527100.

[18] Jahdi S, Alatise O, Fisher C, Ran Li, Mawby P. An evaluation of silicon carbide unipolar technologies for electric vehicle drive-trains. IEEE J Emerg Sel Top Power Electron 2014;2:517–28. https://doi.org/10.1109/JESTPE.2014.2307492.

[19] Tekgun B, Boynuegri AR, Chowdhury M. A., Sozer Y. Design and implementation of a sinusoidal flux controller for core loss measurements. 2016 IEEE Applied Power Electronics Conference and Exposition (APEC), IEEE; 2016, p. 207–14. https://doi.org/10.1109/APEC.2016.7467874.

[20] Holz M, Hultsch G, Scherg T, Rupp R. Reliability considerations for recent Infineon SiC diode releases. Microelectron Reliab 2007;47:1741–5. https://doi.org/10.1016/j.microrel.2007.07.031.

[21] Dubarry M, Devie A, McKenzie K. Durability and reliability of electric vehicle batteries under electric utility grid operations: Bidirectional charging impact analysis. J Power Sources 2017;358:39–49. https://doi.org/10.1016/j.jpowsour.2017.05.015.

[22] Tsoleridis C, Chatzimisios P, Fouliras P. Vehicle-to-Grid Networks: Issues and Challenges. Smart Grid, CRC Press 2016:347–69. https://doi.org/10.1201/b19664-19.

[23] Kempton W, Tomić J. Vehicle-to-grid power fundamentals: Calculating capacity and net revenue. J Power Sources 2005;144:268–79. https://doi.org/10.1016/j.jpowsour.2004.12.025.

[24] Nasr M, Gupta K, da Silva C, Amon CH, Trescases O. SiC based on-board EV power-hub with high-efficiency DC transfer mode through AC port for vehicle-to-vehicle charging. 2018 IEEE Applied Power Electronics Conference and Exposition (APEC), IEEE; 2018, p. 3398–404. https://doi.org/10.1109/APEC.2018.8341591.

[25] Ahmed NA, Alajmi BN, Abdelsalam I, Marei MI. Soft switching multiphase interleaved boost converter with high voltage gain for EV applications. IEEE Access 2022;10:27698–716. https://doi.org/10.1109/ACCESS.2022.3157050.

[26] Alajmi BN, Abdelsalam I, Marei MI, Ahmed NA. Two stage single-phase EV on-board charger based on interleaved cascaded non-inverting buck-boost converter. In: 2023 IEEE Conference on Power Electronics and Renewable Energy (CPERE), IEEE; 2023. p. 1–6. https://doi.org/10.1109/CPERE56564.2023.10119584.

[27] Sousa TJC, Monteiro V, Fernandes JCA, Couto C, Melendez AAN, Afonso JL. New perspectives for vehicle-to-vehicle (V2V) power transfer. In: IECON 2018–44th Annual Conference of the IEEE Industrial Electronics Society; 2018. p. 5183–8. https://doi.org/10.1109/IECON.2018.8591209.

[28] Li H, Sun Y, Wang S, Zhang Z, Ren X, Zhang P, et al. Bidirectional control with fitting model-based synchronous rectification and input ripple current feedforward for SiC bidirectional CLLC EV charger. IEEE Trans Ind Electron 2023;70:9136–46. https://doi.org/10.1109/TIE.2022.3212382.

[29] Khaligh A, D'Antonio M. Global trends in high-power on-board chargers for electric vehicles. IEEE Trans Veh Technol 2019;68:3306–24. https://doi.org/10.1109/TVT.2019.2897050.

[30] IEEE Standards Association. 519-2022 - IEEE Standard for Harmonic Control in Electric Power Systems. n.d. https://doi.org/10.1109/IEEESTD.2022.9848440.

[31] Tekgun D, Tekgun B, Alan I. A Modular Three-Phase Buck-Boost Motor Drive Topology. Proceedings - 2020 6th International Conference on Electric Power and Energy Conversion Systems, EPECS 2020 2020:130–5. https://doi.org/10.1109/EPECS48981.2020.9304972.

[32] Tekgun B, Tekgun D, Alan I, Badawy M. Design and Control of a Single Phase DC/Rectified AC/AC Inverter for low THD Applications. 7th International IEEE Conference on Renewable Energy Research and Applications, ICRERA 2018 2018: 424–30. https://doi.org/10.1109/ICRERA.2018.8566841.

[33] Yasa Y, Sozer Y, Garip M. Loss analysis of high speed switched reluctance machine with integrated simulation methods. Int J Appl Electromagn Mech 2018;56: 479–97. https://doi.org/10.3233/JAE-170113.